Mirna M. Saleh
Ahmed Kalzia
Manar Hassan
Muhammad H. Abzal

Department of Chemistry, Faculty of Science, Tishreen University, Lattakia, SYRIA

Synthesis and Characterization of Perovskite Nanoparticles of $Sr_{2.5}Tb_{0.5}CoFeO_7$, $Sr_{2.5}Tb_{0.5}CoCuO_7$

In this study, nanoparticles of $Sr_{2.5}Tb_{0.5}CoFeO_7$ and $Sr_{2.5}Tb_{0.5}CoCuO_7$, which perovskite derivatives belonging to the Ruddlesden–Popper series were synthesized by modify $Sr_3+Co_2O_7$ (which belong to $A_{n+1}B_nO_{3n+1}$ type) throw partial replacement of cobalt (Co) with copper (Cu) or iron (Fe), and the partial replacement of strontium (Sr) with the terbium (Tb). New compounds were prepared by ceramic method according to thermal program with several stages, then were characterized by XRD, SEM, EDX. Results showed that prepared compounds were crystallizing according to a tetragonal structure within the P42/mnm crystal system, particle size of $Sr_{2.5}Tb_{0.5}CoCuO_7$ was 50.27 nm, $Sr_{2.5}Tb_{0.5}CoFeO_7$ 80.97nm. Specific resistance of prepared compounds was determined, results showed that the specific resistance of the $Sr_{2.5}Tb_{0.5}CoCuO_7$ at a temperature of 700°C amounted to 1.45Ω.cm^2 and that of $Sr_{2.5}Tb_{0.5}CoFeO_7$ was 0.86Ω.cm^2. In conclusion, the physical and structural specifications of the prepared compounds qualify them for use in the field of solid fuel cells.

Keywords: Perovskites; Roddlesden–Popper series; Ceramic method; $Sr_{2.5}Tb_{0.5}CoFeO_7$
Received: 08 May 2024; Revised: 29 July 2024; Accepted: 05 August 2024

1. Introduction

Transition metal oxides have occupied a large area of interest in international scientific research in the recent decades due to the connection between these materials and the most important scientific developments in the field of solid-state chemistry and physics, especially mixed oxides belonging to the perovskite categories and the derived crystal structures due to the important properties that these oxides possess in addition to their potential technological applications. In the recent years, two major events provoked scientific interest in studying the magnetic properties and electrical transport of these materials; the first was discovering the high-temperature superconductivity of mixed copper oxides with a structure derived from the perovskite structure [1] and the second is the recent discovery of large values of negative magnetoresistance in perovskites of mixed valence magnesium oxides [2].

Compounds belonging to the Ruddlesden-Popper series are metal oxides that have occupied a large area of interest in the field of solid chemistry and physics because of important physical properties they have such as electrical insulation [3] $Sr_{n+1}TinO_{3n+1}$, superconductivity [4] $Sr_{n+1}RunO_{3n+1}$ and magnetoresistance [5] $Sr_{n+1}MnnO_{3n+1}$.

The structure of the compounds belonging to Ruddlesden-Popper series is derived from the structure of perovskite which ideal structure can be described with the formula ABO_3 as a cubic crystal structure formed by the presence of B ions in the center of the octahedrons that are connected to each other by the vertices, while the A ions are present in the center of the polyhedron As shown in Fig. (1), B ions are located at the vertices of the cube and A ions are located in its center while oxygen ions are located in the middle of the sides of the cube. We note that ion B has a coordination number equal to six and ion A has a coordination number equal to 12 by oxygen ions. Therefore, the crystal structure of these compounds consists of octahedra [BO_6] that share a cubic position at the vertices with ions in the cubic spaces of the octahedral [6-8].

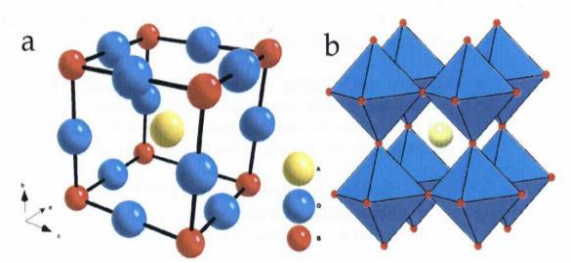

Fig. (1) The ideal structure of perovskite ABO_3 [6]

There are a large number of compounds associated with the perovskite structure. Compounds of this type are called layered perovskites where perovskite consists of infinite 2D plane layers of the ABX_3 type that are repeatedly separated.

Accordingly, three widely studied structural chains were identified and named after the names of the first researchers, which are:

1- Ruddlesden-Popper series
2- Dyne-Maxon series
3- Arevilius series

In this work, we study the compounds of the Ruddlesden-Popper series that have the general formula of $(AO)(ABO_3)_n$ [9]. Members of the Ruddlesden-Popper series are structurally characterized by the growth of perovskite layers composed of n octahedrons [BO_6] along the crystal axis c that appear separated by layers with a sodium chloride [A_2O_2] type structure, thus producing a series of compounds belonging to the Ruddlesden-Popper family $(AO)(ABO_3)_n$. For n=1, we obtain the compounds A_2BO_4, and for n=2, we obtain the compounds $A_3B_2O_7$, etc. as shown in Fig. (2a,b) and

when n=∞, we obtain the crystal structure of perovskite as shown in Fig. (2c).

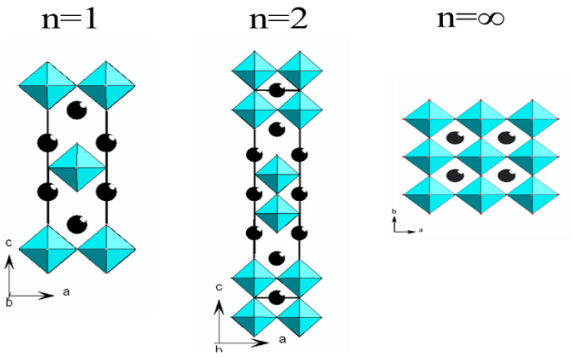

Fig. (2) Crystal structure of compounds belonging to the Ruddlesden-Popper series along c axis [6]

The presence of $[A_2O_2]$ levels distort the three-dimensional morphology of the perovskite structure and gives three important properties to these compounds [10].

- Anisotropy and difference of the physical properties in the plane ab or along the crystal axis c, this is due to structural anisotropy which leads to electronic anisotropy.
- The structural change affects the electrical charge of these compounds. According to their layered structure, they are alternately electrically charged. For example, for the compound $A_2^{+3}B^{+2}O_4$ in the perovskite level $[BO_2]$ the charge is negative (2-), while with layers with structure of sodium chloride type $[A_2O_2]$ the charge is positive (2+). The presence of this internal electric field causes the stability of electronic energy levels in the positively charged areas and destroys their stability in the negatively charged areas.
- When the ionic radius of cations A and B is smaller or larger than the size of the corresponding vacancies in the crystal structure, an internal voltage on the layers of the crystal structure is created causing deformation of the crystal structure.

Compounds at n=1 form mixed oxides with the general formula A_2BO_4 which are the most studied compounds in the Ruddlesden-Popper family as the ideal crystalline structure of these compounds crystallizes according to the structural model of the compound K_2NiF_4 within the tetragonal quaternary system according to the steric symmetry I4/mmm. Cations B have its coordination number equal to six, while the cations of the A crystal site have a coordination number equal to nine by oxygen ions. It is clear that compared to the perovskite structure, the coordination of the A cation is reduced.

At n=2, the compounds form mixed oxides with the general formula $A_3B_2O_7$. The ideal crystal structure for these compounds crystallize according to the structural model of the compound $Sr_3Ti_2O_7$ within the tetragonal quaternary system according to the symmetry I4/mmm, or they crystallize within the tetragonal quaternary system according to the symmetry P42/mnm according to the structural model $Eu_2SrFe_2O_7$.

In these compounds, the A cations are located in two layers; a layer with a perovskite structure and a layer with a NaCl structure in two different arrangements as the cations that are in the perovskite layers are located in a coordination number of 12, while those located in a coordination number of 9 are in the layers that have a NaCl structure.

The stability of the perovskite structure and its derived structures is mainly related to the tendency of cation B to achieve octet conformation and for cation A to be large. The lower bounds on the radii of cations A and B that can occupy cationic sites are (radius A: 0.9Å) and (radius B: 0.51Å). If the radius of ion B is less than this value, the lengths of its bonds with oxygen will change, and therefore the octahedron will be unstable. To achieve stability of the structure, cation B forms a bond number less than the octahedra. An equation explaining the nature of the relationship between the ionic radii of these elements in order to achieve a stable crystalline structure was reached [11], and it is known as the tolerance factor:

$$t = \frac{r_A + r_O}{\sqrt{2}(r_B + r_O)} \quad (1)$$

where r_A is the radius of cation A, r_B is the radius of cation B, and r_O is the radius of ion O. If t=1, the crystal structure is a perfect cubic structure without any distortion because the ionic radii of A and B exactly match the radius of their gaps in the crystal lattice.

When the value of t decreases, the crystal structure undergoes stress (tension and compression) of the bonds, such that the B-O bonds are subject to compressive forces and the A-O bonds to tensile forces as a result of the Jahn-Teller action. To relieve these tensions, distortions occur in the structure, which leads to a decrease in its symmetry.

Through the study conducted on compounds belonging to the Ruddlesden-Popper series, it was noted that the dimensions of the crystal structure of these compounds are related to the electrical resistance, noting that the crystal structure of the compounds when n=∞ (perovskite structure) is three-dimensional (3D) and the crystal structure of the compounds when n=1 (the K_2NiF_4 structure) is two-dimensional (2D), and for the rest of the compounds belonging to the RP series when n≥2 their crystal structure is between three-dimensional and two-dimensional depending on the value of n [12,13].

This means that by reducing the dimensions of the crystal lattice, the electrical resistance increases. For example: In the family of compounds $(La/Sr)_{n+1}Mn_nO_{3n+1}$ (n=1, 2, and ∞), at the same degree of partial replacement of all compounds, the compound with crystal 3D perovskite structure shows conductive behavior while the compound at n=1 with 2D structure shows the behavior of semiconductors and the compound at n=2 shows the behavior of insulators with its electrical resistance

value averages between the resistance values of perovskite compounds and n=1 compounds [14-16].

Among the most important compounds that belong to the Ruddlesden-Popper series at (n=2) that were studied are the cobalt compounds $Gd_2SrCo_2O_7$, $Sr_2SmCo_2O_7$, and $Sm_2BaCo_2O_7$. It was shown in these compounds that cobalt has an oxidation degree of (3+) and crystallizes according to the structural model of the compound $Sr_3Ti_2O_7$ within the tetragonal quaternary system according to the I4/mmm symmetry. The magnetic and electrical properties of these compounds were studied and showed paramagnetic and semiconductor behavior [17]. The compound $Eu_2SrCo_{1.5}Fe_{0.5}O_7$ was synthesized at a temperature of 1250°C. This compound crystallized within the tetragonal quaternary system according to the symmetry P42/mnm [18].

The aim of this study is to modify $Sr_3+Co_2O_7$ perovskite derivatives belonging to the Ruddlesden–Popper series of the type $A_{n+1}B_nO_{3n+1}$ by partial replacement of cobalt (Co) with copper (Cu) and iron (Fe), and the partial replacement of strontium (Sr) with the terbium (Tb) to obtain new nanostructures of $Sr_{2.5}Tb_{0.5}CoFeO_7$ and $Sr_{2.5}Tb_{0.5}CoCuO_7$, then study properties of the resulting compounds.

2. Materials and Methods

Nanoparticles of $Sr_{2.5}Tb_{0.5}CoFeO_7$, $Sr_{2.5}Tb_{0.5}CoCuO_7$ were synthesized using the ceramic method, the chemicals in the experiment were analytical grade and used without further purification, the following materials were used: strontium carbonate $SrCO_3$, copper oxide CuO, terbium oxide Tb_4O_7, $Fe(NO_3)_3$ and cobalt oxide Co_2O_3 all from (Aladdin Chemistry Co., Ltd.).

The raw materials were weighed by TE 64-Sartorius according to the stoichiometric ratios of the atoms within the compound formulas, mixtures were ground in an agate pestle to obtain greater homogeneity, then heated in an incineration furnace (Carbolite, Bamford, Sheffiejd, England, S30 2AU) according to the thermal program in table (1).

The properties and structure of the prepared nanoparticles was studied by X-ray diffractometer XRD (Bruker AXSD8 Focus), scanning electron microscopy (HITACHI S4800 microscope Chiyoda-ku, Japan) linked to an EDX/INCA 350 (energy dispersive X-ray analyzer) manufactured by Oxford Instruments Ltd. (UK). Nodular impedance and electrical conductivity were measured in the frequency range 0.1-1000 Hz. When plotting $Z'(\Omega.cm^2)$ with $-Z''(\Omega.cm^2)$, we get a semicircle, one end of which represents the resistance of the pellet and the other represents the resistance of the pellet and its boundaries.

3. Results and Discussion

Throughout XRD patterns of the prepared compound based on the High Score Plus program with dimensions and Miller's hkl indices for each peak, the results show that the prepared compounds were formed at a temperature of 1050°C for 48 h according to the quaternary structure (Tetragonal p42/mnm), as shown in Fig. (3), Fig. (4), and table (2).

Table (1) Thermal program for prepare the samples

Time (hours)	Temperature (°C)
2	100/105
3	700
48	900
48	950
48	1050

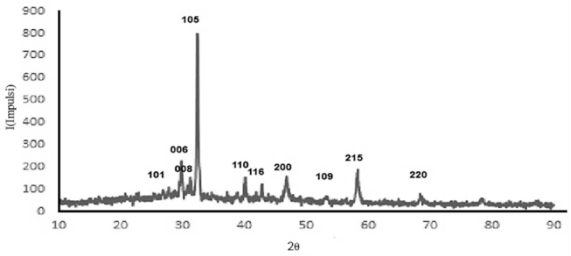

Fig. (3) XRD pattern of $Sr_{2.5}Tb_{0.5}CoCuO_7$ sample

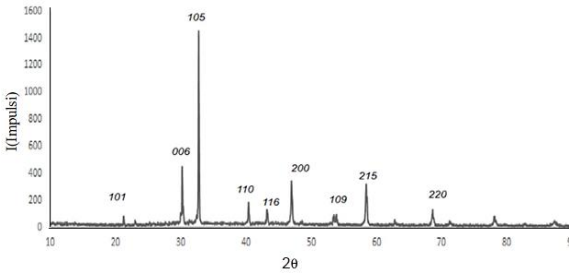

Fig. (4) XRD pattern of $Sr_{2.5}Tb_{0.5}CoFeO_7$ sample

It was noted from results in table (2) that when the cobalt was partially replaced with copper and iron and at the same time the strontium is partially replaced with terbium, there was a difference in the values of the cell parameters (a, b, c) compared to the basic compound $Sr_3Co_2O_7$ [19] and the compound Sr_3CoCuO_7, where deformation of the octahedron occurs due to the difference in radii of the elements Fe, Cu, and Co, $r(Fe^{+2})=0.75Å$, $r(Cu^{+2})=0.87Å$, $r(Co^{+2})=0.79Å$. Partial replacement at site A also leads to distortion within the crystal lattice as a result of the difference in ionic radii between strontium and terbium. Comparing the results from table (2) the grain size and degree of crystallinity when partial replacement with iron was smaller because the ionic radius of iron is smaller than that of copper.

Elemental composition of surface of prepared $Sr_{2.5}Tb_{0.5}CoCuO_7$ by EDX shown in Fig. (5) shows presence of the terbium element corresponding to the TbM_α transition corresponding to the value 1.1keV, and the OK_α transition corresponding to the oxygen element corresponding to the value 0.55keV, which belongs to the oxides involved in the oxide composition. It also shows the copper element corresponding to the two transitions CuK_α and CuK_α

corresponding to the values 7.4 and 8.2 keV, respectively, and the cobalt element corresponding to the two transitions CoKα and CoKα corresponding to the values 6.85 and 7.41 keV, respectively. The strontium element corresponding to the two transitions SrLα and SrLα corresponding to the values 1.9 and 1.85 keV, respectively, were also shown.

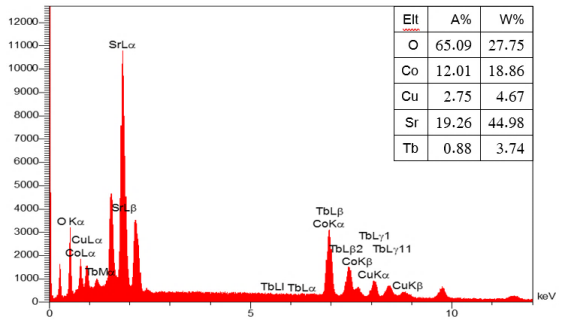

Fig. (5) EDX spectrum of prepared $Sr_{2.5}Tb_{0.5}CoCuO_7$

The elemental composition of the surface of prepared $Sr_{2.5}Tb_{0.5}CoFeO_7$ sample shown in Fig. (6) shows the presence of the terbium element corresponding to the TbMα transition corresponding to the value 2.9keV and the OKα transition corresponding to the oxygen element corresponding to the value 0.53keV, which belongs to the oxides involved in the oxide structure. Also, the iron element was shown corresponding to the two transitions, FeKα and FeKα corresponding to the values 6.8 and 6.4 keV, respectively. The cobalt corresponding to the transitions CoKα and CoKα corresponding to the values 6.9 and 7.3 keV, respectively, is shown in addition to the strontium corresponding to the transitions SrLα and SrLα, corresponding to the values 1.91 and 1.83 keV, respectively.

From Fig. (5) and Fig. (6), we notice that the atomic distribution ratio of the elements in the prepared compounds corresponds to the stoichiometric ratios of the atoms in the studied compound. It also notice the difference in the locations of the peaks as a result of the difference in the dopant element which affects the dimensions of the crystal and the grain size of the two prepared compounds.

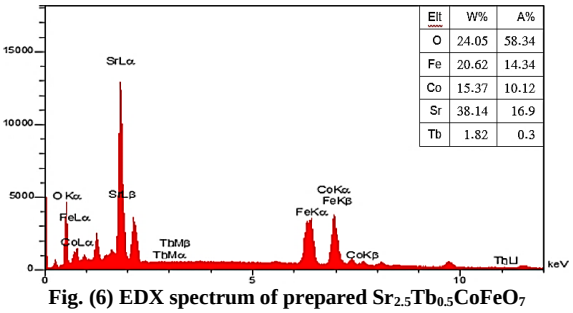

Fig. (6) EDX spectrum of prepared $Sr_{2.5}Tb_{0.5}CoFeO_7$

Scaning electron microscope (SEM) images of prepared samples in Fig. (7) and Fig. (8) show the presence of huge and large aggregates in the prepared sample in (Fig. 8) compared to (Fig. 7) due to the difference between the ionic radii of iron and copper. The average particle size of the prepared samples was studied based on the Digimizer program and that the two compounds were in nano-sized $Sr_{2.5}Tb_{0.5}CoFeO_7$ was 50.27nm, $Sr_{2.5}Tb_{0.5}CoCuO_7$ was 80.97nm.

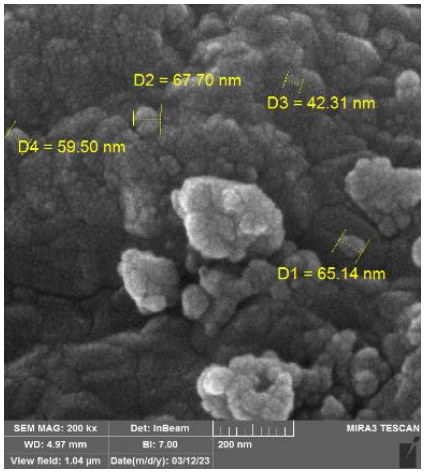

Fig. (7) SEM image of the $Sr_{2.5}Tb_{0.5}CoCuO_7$ sample

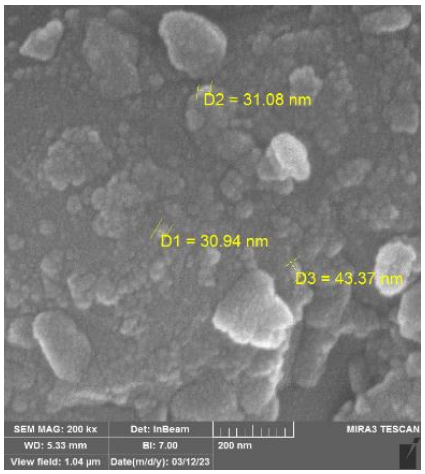

Fig. (8) SEM image of the $Sr_{2.5}Tb_{0.5}CoFeO_7$ sample

Figures (9) and (10) show that the distribution ratio of atoms on the surface of the samples were consistent with the EDX analysis of the prepared compounds.

Impedance were measured in the frequency range 0.1-1000 Hz. When plotting Z'(Ω.cm^2) with -Z"(Ω.cm^2) we get a semicircle, one end of which represents the resistance of the pellet and the other represents the resistance of the pellet and its boundaries, as shown in the Nyquist diagram in figures (11) and (12). Value of R.δ was found using the EC-LAB program and the conductivity value of the compound $Sr_{2.5}Tb_{0.5}CoCuO_7$ was 0.68 Ω.cm^2 and its specific resistance was 1.45 Ω.cm^2. The conductivity value of the compound $Sr_{2.5}Tb_{0.5}CoFeO_7$ was 1.16 Ω.cm^2 and its specific resistance was 0.86 Ω.cm^2.

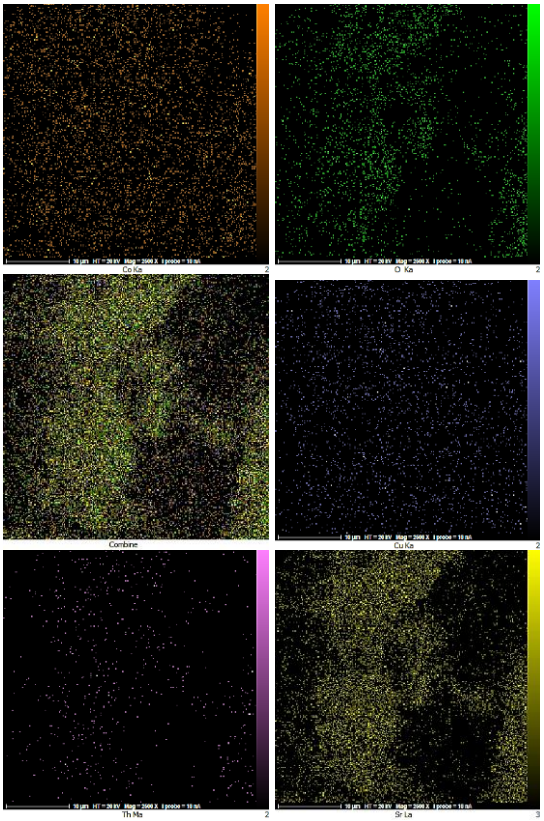

Fig. (9) SEM mapping images of $Sr_{2.5}Tb_{0.5}CoCuO_7$ sample

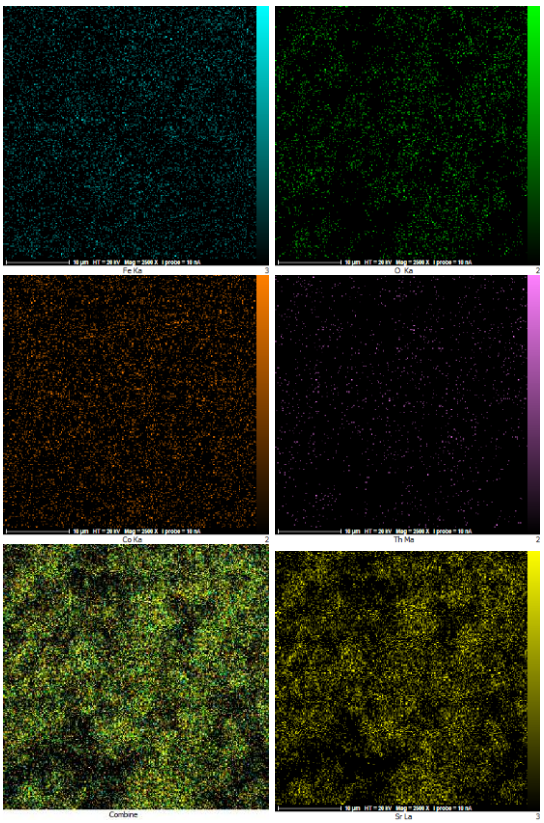

Fig. (10) SEM mapping images of $Sr_{2.5}Tb_{0.5}CoFeO_7$ sample

The prepared compounds behave as conductors of electric current, as these compounds show a greater resistance value compared to the $La_{0.25}Sr_{2.75}FeNiO_{7-\delta}$ compound, which showed a specific resistance of 0.26 Ω.cm^2 and a lower value with the $La_3Ni_2O_{7-\delta}$ compound with resistance of 7.6 Ω.cm^2 [20,21]. Comparing the results of the specific conductivity and specific resistance of the two compounds, we note that the specific resistance is higher in the compound $Sr_{2.5}Tb_{0.5}CoCuO_7$. This was due to the degree of crystallinity, the particle size, and the larger crystalline size of this compound, which were consistent with the results shown in table (2), tables (3), Fig. (10), and Fig. (11).

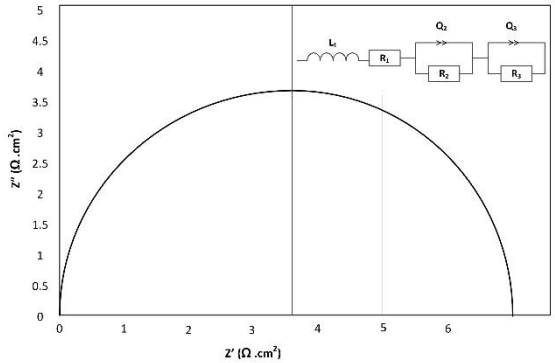

Fig. (11) Nyquist curve for $Sr_{2.5}Tb_{0.5}CoCuO_7$ sample

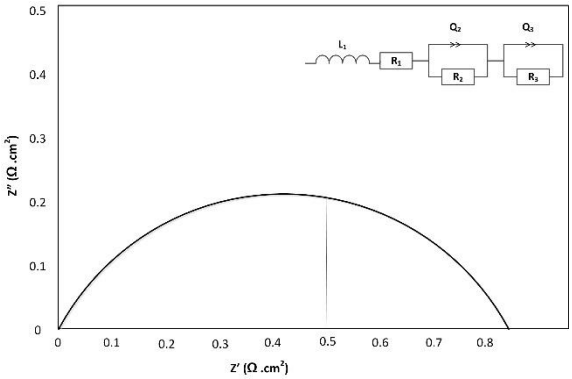

Fig. (12) Nyquist curve for $Sr_{2.5}Tb_{0.5}CoFeO_7$ sample

4. Conclusions

Nanoparticles of $Sr_{2.5}Tb_{0.5}CoFeO_7$ and $Sr_{2.5}Tb_{0.5}CoCuO_7$ were synthesized by modify $Sr_3+Co_2O_7$ perovskite derivatives belonging to the Ruddlesden–Popper series the type $A_{n+1}B_nO_{3n+1}$ by partial replacement of cobalt with copper and iron, and the partial replacement of strontium with the terbium.

Nanoparticles of $Sr_{2.5}Tb_{0.5}CoFeO_7$ and $Sr_{2.5}Tb_{0.5}CoCuO_7$ were synthesized by the ceramic method and the prepared compounds were crystallizing according to a tetragonal structure within the P42/mnm crystal system, particle size of $Sr_{2.5}Tb_{0.5}CoCuO_7$ was 80.97nm, $Sr_{2.5}Tb_{0.5}CoFeO_7$ 50.27 nm. Specific resistance of prepared compounds was determined, results showed that the specific resistance of the $Sr_{2.5}Tb_{0.5}CoCuO_7$ at a temperature of 700°C amounted to 1.45 Ω.cm^2 and that of $Sr_{2.5}Tb_{0.5}CoFeO_7$ was 0.86 Ω.cm^2. In conclusion, the physical and structural specifications of the prepared

compounds qualify them for use in the field of solid fuel cells.

Acknowledgement

The authors would like to thank Tishreen University, Latakia, Syria.

References

[1] Y. Wang et al., "Photocatlytic degradation of simulated dye wastewater in different pH environments by using $BaTiO_3/Bi_2WO_6$ heterojunction photocatalysts", *Opt. Mater.*, 113 (2021) 110853.

[2] L. Ning et al., "Catalytic membrane-based oxidation-filtration systems for organic wastewater purification: A review*", J. Hazard. Mater*., 414 (2021) 125478.

[3] D. Jaspal and A. Malviya, "Composites for wastewater purification: A review", *Chemosphere*, 246 (2020) 125788.

[4] S.H.S. Chan et al., "Recent developments of metal oxide semiconductors as photocatalysts in advanced oxidation processes (AOPs) for treatment of dye wastewater*", J. Chem. Technol. Biotechnol*., 86 (2011) 1130–1158.

[5] S. Labrim et al., "Strain Effect on Optoelectronic and Thermoelectric Properties of the Perovskite $NaGeI_3$", *Spin*., 14(3) (2024) 2450003.

[6] M. Shatruk and J.K. Clark, **"Magnetic Materials"**, Elsevier eBooks (2023) 236–261.

[7] M.A. Yatoo and S.J. Skinner, "Ruddlesden-Popper phase materials for solid oxide fuel cell cathodes: A short review", *Mater. Today: Proc.*, 56(6) (2022) 3747-3754.

[8] X. Xu et al., "Ruddlesden–Popper perovskites in electrocatalysis" *Mater. Horizons.*, 7(10) (2020) 2519–2565.

[9] M.P. Arciniegas and L. Manna, "Designing Ruddlesden–Popper Layered Perovskites through Their Organic Cations", *ACS Energy Lett*., 7(9) (2022) 2944–2953.

[10] S. Li and T. Birol, "Suppressing the ferroelectric switching barrier in hybrid improper ferroelectrics", *npj Comput. Mater*., 6(1) (2020) doi: 10.1038/s41524-020-00436-x

[11] L.H. Omari et al., "Structural and optical properties of Fe-doped Ruddlesden-Popper $Ca_3Ti_{2-x}Fe_xO_{7-\delta}$ nanoparticles", *Mater. Chem. Phys*, 246 (2020) 122810.

[12] B. Liu et al., "Synthesis, crystal structure and microwave dielectric properties of $Sr_2LnMgNbO_7$ (Ln=La,Nd,Sm) novel compounds with Ruddlesden-Popper structure", *Mater. Lett*., 238 (2019) 245.

[13] G.J. Li et al., "Crystal structural evolution and hybrid improper ferroelectricity in Ruddlesden-Popper $Ca_{3-x}Sr_xTi_2O_7$ ceramics", *Appl. Phys. Lett*., 123 (2018) 014101.

[14] L.H. Omari et al., "Structural and optical properties of Fe-doped Ruddlesden-Popper $Ca_3Ti_{2-x}Fe_xO_{7-\delta}$ nanoparticles", *Mater. Chem. Phys*., 246 (2020) 122810.

[15] T. Dawa and B. Sajjadi, "Exploring the potential of perovskite structures for chemical looping technology: A state-of-the-art review", *Fuel Process. Technol*, 53 (2024) 108022.

[16] J. Song et al., "Structure, electrical conductivity and oxygen transport properties of Ruddlesden–Popper phases $Ln_{n+1}Ni_nO_{3n+1}$ (Ln=La, Pr and Nd; n=1, 2 and 3)", *J. Mater. Chem. A*, 8(42) (2020) 22206–22221.

[17] M. Garali et al., "Synthesis, characterization and electrochemical properties of $La_{2-x}Eu_xNiO_{4+\delta}$ Ruddlesden-Popper-type layered nickelates as cathode materials for SOFC applications", *Int. J. Hydrog. Ener.*, 44(21) (2019) 11020–11032.

[18] L. Malavasi, M. Karlsson and M. Coduri, "Structure–property correlation in oxide-ion and proton conductors for clean energy applications: recent experimental and computational advancements", *J. Mater. Chem. A*., 10(10) (2022) 5082–5110.

[19] I. Qadir et al., "Synthesis of Ruddlesden-Popper $LaSrFe_{1-x}Cr_xO_4$ phases (x = 0.0, 0.2, 0.4, 0.6) by glycine-nitrate combustion process: Effect of Cr doping on magnetic, optical and photocatalytic properties", *J. Alloys Comp*., 920 (2022) 165865.

[20] M. Mousavi, T. Ghorbani-Moghadam and A. Kompany, "Investigation of methyl orange photocatalytic degradation using $La_{0.7}Sr_{1.3}CoO_4$ Ruddlesden-Popper nanoparticles", *Ceram. Int.*, 47(14) (2021) 20651-20658.

[21] L. Fang et al., "Comparative investigation of piezocatalysts composed of La, Sr and Co (Fe) complex oxides in Ruddlesden-Popper type or simple single perovskites for efficient hydrogen peroxide generation", *Chem. Eng. J*., 461 (2023) 141866.

Table (2) Granular size and degree of crystallinity with cell dimensions for prepared compounds

Prepared compound	a(Å)=b(Å)	c(Å)	Granular size D(nm)	Degree of crystallinity (nm)
$Sr_{2.5}Tb_{0.5}CoFeO_7$	3.42	23.92	44.90	29.56
$Sr_{2.5}Tb_{0.5}CoCuO_7$	3.92	21.13	73.74	48.42

